FED-Vol. 123, Advances in Finite Element
Analysis in Fluid Dynamics
ASME 1991

FINITE ELEMENT COMPUTATION OF COMPRESSIBLE FLOWS WITH THE SUPG FORMULATION†

G. J. Le Beau
Navigation Control and Aeronautics Division
NASA–Johnson Space Center
Houston, Texas

T. E. Tezduyar
Department of Aerospace Engineering and Mechanics
Minnesota Supercomputer Institute
University of Minnesota
Minneapolis, Minnesota

ABSTRACT

Finite element computation of compressible Euler equations is presented in the context of the streamline-upwind/Petrov-Galerkin (SUPG) formulation. The SUPG formulation, which is based on adding stabilizing terms to the Galerkin formulation, is further supplemented with a shock capturing operator which addresses the difficulty in maintaining a satisfactory solution near discontinuities in the solution field. The shock capturing operator, which has been derived from work done in entropy variables for a similar operator, is shown to lead to an appropriate level of additional stabilization near shocks, without resulting in excessive numerical diffusion. An implicit treatment of the impermeable wall boundary condition is also presented. This treatment of the no-penetration condition offers increased stability for large Courant numbers, and accelerated convergence of the computations for both implicit and explicit applications. Several examples are presented to demonstrate the ability of this method to solve the equations governing compressible fluid flow.

INTRODUCTION

The physics and dynamics of problems involving compressible flows in aerospace applications are not yet fully understood. Particularly, better understanding of dynamical, thermal, and chemical aspects of the reentry conditions is needed. While the prediction of aerodynamic and heating loads is very important for designing space vehicles (Li, 1986), the conditions, such as altitude and speed, under which space vehicles operate makes the simulation by ground test facilities extremely difficult. Therefore, computational predictions based on the solution of the appropriate governing equations have become crucial.

Thus, the objective of this work is to address issues associated with solving compressible flow problems using the finite element method. While it is hoped that the inherent flexibility of the finite element method to model complicated geometries will enable engineers to model flows past such vehicles as the Space Shuttle and the Aeroassist Flight Experiment, this research has concentrated on developing effective strategies for the solution of compressible flows in two dimensions, which can then be extended to more complex three-dimensional problems.

Among the difficulties associated with numerical simulation of compressible flows is the treatment of shocks and sharp layers. For high-speed flows, the magnitude of such sharp variations in the flow field can be very large, making the computation even more challenging. It is well known that Galerkin finite element (or classical central difference) schemes result in spurious oscillations for advection-dominated problems due to their hyperbolic nature, especially in the presence of sharp layers in the solution. To minimize such effects, a streamline-upwind/Petrov-Galerkin (SUPG) formulation is employed. Such schemes, which introduce minimal numerical diffusion, have been successfully applied to various fluid dynamics problems (Brooks and Hughes, 1982; Tezduyar and Hughes, 1982; Tezduyar and Hughes, 1983; Tezduyar *et al.*, 1988). Furthermore, to obtain better solutions in the presence of shocks, a discontinuity capturing scheme was

† This research was sponsored by the NASA-Johnson Space Center (grant NAG 9-449), NSF (grant MSM-8796352) and the University of Minnesota Army High Performance Computing Research Center.

incorporated (Hughes *et al.*, 1986; Hughes and Mallet, 1986). Such schemes are designed to introduce a dissipative effect in the neighborhood of discontinuities, without degrading the accuracy of the solution elsewhere in the flow field.

When numerically solving the compressible Euler equations, the implementation of the impermeable wall boundary condition requires special attention. Traditionally, an explicit implementation of this boundary condition has been used at solid surfaces through a flux-vector manipulation at the surface. Because this explicit treatment of the boundary condition adversely affects the stability properties of an implicit method, we have implemented an implicit treatment of this situation. In the formulation of this boundary condition, the normal and tangential components of the momentum are kept track of, rather than the Cartesian components. The normal component of the momentum can then be set to zero as a Dirichlet boundary condition. Translation between the normal-tangential components frame and the Cartesian components frame is accomplished by using a local transformation rule, dependent on the geometry of the boundary.

GOVERNING EQUATIONS

Let Ω be a domain in R^{nsd} and T be a positive real number, where n_{sd} is the number of spatial dimensions. The spatial and temporal coordinates are denoted by $\mathbf{x} \in \bar{\Omega}$ and $t \in [0,T]$, where a superposed bar indicates the set closure. The boundary of the domain Ω is denoted by Γ. The dynamics which governs multi-dimensional inviscid, compressible fluid flow are described by the Euler equations. These equations, written in terms of conservation variables $\mathbf{U} = (\rho, \rho u_1, ..., \rho u_{nsd}, \rho e)^T$, are

$$\frac{\partial \mathbf{U}}{\partial t} + \frac{\partial \mathbf{F}_i}{\partial x_i} = 0 \qquad \text{on } \Omega \times (0,T), \tag{1}$$

where $\mathbf{F}_1, ..., \mathbf{F}_{nsd}$ are the Euler fluxes, and repeated indices imply summation over the range of the spatial dimension n_{sd}. Alternatively, equation (1) can be written as

$$\frac{\partial \mathbf{U}}{\partial t} + \mathbf{A}_i \frac{\partial \mathbf{U}}{\partial x_i} = 0 \qquad \text{on } \Omega \times (0,T), \tag{2}$$

where

$$\mathbf{A}_i = \frac{\partial \mathbf{F}_i}{\partial \mathbf{U}}, \; i = 1, ..., n_{sd}. \tag{3}$$

We assume that associated with (2), the following boundary and initial conditions are given;

$$\mathbf{B}\,\mathbf{U} = \mathbf{G} \qquad \text{on } \Gamma \times (0,T), \tag{4}$$

$$\mathbf{U}(\mathbf{x},0) = \mathbf{U}_0(\mathbf{x}) \qquad \text{on } \Omega, \tag{5}$$

where $\mathbf{B}$ denotes a general boundary operator, and $\mathbf{G}$ and $\mathbf{U}_0$ are given functions. Because the Euler equations neglect the viscous terms of the Navier-Stokes equations, the flow is allowed to slip at a solid surface. However, for obvious reasons, there should be no flow penetration at the surface. Thus at each point on the surface, the solution of an Eulerian flow must satisfy

$$u_i \, n_i = 0, \tag{6}$$

where n_i, $i = 1, ..., n_{sd}$ are the components of the unit normal vector vector.

FINITE ELEMENT FORMULATION

Consider a finite element discretization of the domain Ω into subdomains (elements) Ω^e, $e = 1, 2, ..., n_{el}$ where n_{el} is the number of elements. Throughout, we shall assume that the trial solution $\mathbf{U}$ satisfies $\mathbf{B}\,\mathbf{U} = \mathbf{G}$ on Γ. Furthermore, the weighting function $\mathbf{W}$ satisfies $\mathbf{B}\,\mathbf{W} = \mathbf{0}$ on Γ. We define the following function spaces:

$$S^h = \{ \mathbf{U}^h | \mathbf{U}^h \in [H^{1h}(\Omega)]^{ndof}, \; \mathbf{U}^h|_{\Omega^e} \in [P^1(\Omega^e)]^{ndof}, \; \mathbf{B}\mathbf{U}^h \doteq \mathbf{G} \text{ on } \Gamma \}, \tag{7}$$

$$V^h = \{ \mathbf{W}^h | \mathbf{W}^h \in [H^{1h}(\Omega)]^{ndof}, \; \mathbf{W}^h|_{\Omega^e} \in [P^1(\Omega^e)]^{ndof}, \; \mathbf{B}\mathbf{W}^h \doteq \mathbf{0} \text{ on } \Gamma \}, \tag{8}$$

where n_{dof} is the number of degrees of freedom. The finite element formulation of the Euler equations can be written as follows: find $\mathbf{U}^h \in S^h$ such that $\forall \mathbf{W}^h \in V^h$

$$\int_\Omega \mathbf{W}^h \cdot \left(\frac{\partial \mathbf{U}^h}{\partial t} + \mathbf{A}_i \frac{\partial \mathbf{U}_h}{\partial x_i} \right) d\Omega +$$

$$\sum_{e=1}^{nel} \int_{\Omega^e} \tau \, \mathbf{A}_i^T \frac{\partial \mathbf{W}^h}{\partial x_i} \cdot \left(\frac{\partial \mathbf{U}^h}{\partial t} + \mathbf{A}_i \frac{\partial \mathbf{U}_h}{\partial x_i} \right) d\Omega +$$

$$\sum_{e=1}^{nel} \int_{\Omega^e} \delta \, \frac{\partial \mathbf{W}^h}{\partial x_i} \frac{\partial \mathbf{U}_h}{\partial x_i} \, d\Omega = 0, \tag{9}$$

where the first integral represents the Galerkin formulation, the second one is the SUPG stabilization term, and the last integral is the shock capturing term. The significance of the SUPG formulation is that it adds numerical stability to the standard Galerkin method. While the use of SUPG stabilization alone works quite well for

advection-dominated flows, as the Mach number increases into the supersonic range, the presence of over- and under-shoot in the area of shocks is apparent. Such oscillations, which initially appear in transonic flows, become detrimentally large as the Mach number increases. To alleviate this problem the shock capturing term was added to the formulation.

In this formulation τ is defined as

$$\tau = \max (\tau_i , i = 1 \text{ to } n_{dof}) , \tag{10}$$

where

$$\tau_i , = \frac{\alpha \, h_i}{\rho_i} , \quad (no\ sum). \tag{11}$$

Here h_i is the element length in the x_i direction, α is a parameter controlling the stability and accuracy of the time-integration algorithm, and ρ_i is the spectral radius of $\mathbf{A}_i$ (Tezduyar and Hughes, 1982). That is

$$\rho_i = \max_{1 \le j \le n_{dof}} | \lambda_j (\mathbf{A}_i) | , \tag{12}$$

where the $\lambda_j(\mathbf{A}_i)$'s are the eigenvalues of $\mathbf{A}_i$ which has rank n_{dof}. We define the shock capturing operator for conservation variables as

$$\delta = \left[\frac{\mathbf{A}_i \frac{\partial \mathbf{U}}{\partial x_i} \cdot \tilde{\mathbf{A}}_0^{-1} \mathbf{A}_j \frac{\partial \mathbf{U}}{\partial x_j}}{\frac{\partial \xi_l}{\partial x_j} \frac{\partial \mathbf{U}}{\partial x_j} \cdot \tilde{\mathbf{A}}_0^{-1} \frac{\partial \xi_l}{\partial x_k} \frac{\partial \mathbf{U}}{\partial x_k}} \right]^{1/2} , \tag{13}$$

where $\tilde{\mathbf{A}}_0$ is the Jacobian matrix of the transformation from entropy variables to conservation variables. We derived (13), by a reverse transformation, from the shock capturing operator given for the entropy variables (Hughes and Mallet, 1986).

SOLID WALL BOUNDARY CONDITION

In the past, typical implementation of the boundary condition given by (6) has involved manipulation of the velocity vectors such that the advection normal to the surface is zero after each iteration. This has been accomplished by simply killing the normal component of the velocity at the surface, or by rotation of the velocity vector tangent to the surface in an effort to maintain the kinetic energy at each point. These methods of satisfying the boundary condition have been successfully implemented for quite some time, yet it should be realized that this is an explicit treatment of the boundary condition. Thus even when using an implicit method, the stability of the algorithm will be influenced by this explicit treatment of the boundary condition. Herein is a description of the method used for handling the impermeable wall boundary condition.

The success of this implementation is due to the treatment of the solid surface as a Dirichlet boundary which, by definition of the trial space, allows one to dictate that the normal component of the velocity on a stationary surface must be zero. This implicit treatment of the boundary condition has been used to improve the convergence rates of both explicit and implicit algorithms and has also allowed the use of very large Courant numbers, defined as

$$c_{\Delta t} = \max_{(e,i)} \frac{\rho(\mathbf{A}_i) \, \Delta t}{h_i^e} , \tag{14}$$

in the solution of steady-state Eulerian flows.

In the finite element discretization, the quantity $\mathbf{U}$ is determined within each element by the nodal values $\mathbf{U}_B$ and a set of shape or interpolation functions N_B such that

$$\mathbf{U} = \sum_{B=1}^{m} \mathrm{N}_B \, \mathbf{U}_B , \tag{15}$$

where m is the number of nodes in the element. In equation (15) the variable $\mathbf{U}$ is a nodal vector of unknowns based on a Cartesian coordinate system. Such a system does not directly allow enforcement of the requirement that the normal component of the velocity on a surface be zero because it is a geometric combination of the x_1 and x_2 components of the velocity at the surface node. Therefore a new nodal vector of unknowns for surface nodes is defined where the second and third components of this new vector represent components of the velocity in the tangential (τ) and normal ($\mathbf{n}$) directions respectively. This new vector, defined as

$$\mathbf{d} = \begin{pmatrix} \rho \\ \rho u_\tau \\ \rho u_\mathrm{n} \\ \rho e \end{pmatrix} , \tag{16}$$

allows the third degree of freedom to be designated as a Dirichlet boundary and to implicitly specify that the normal component of the momentum be zero.

Although introduction of a local coordinate system permits the direct enforcement of a no penetration

condition, there may be a need for many such coordinate systems depending on the shape and resolution of the surface. Since it is not possible to obtain a solution over a spatial domain where, conceivably, each node may use a separate coordinate system, each of these τ-**n** systems must be rotated to one uniform system. To accomplish this, a nodal rotation matrix, defined as

$$\mathbf{T}^B = \begin{bmatrix} 1 & 0 & 0 & 0 \\ 0 & \cos\theta_B & -\sin\theta_B & 0 \\ 0 & \sin\theta_B & \cos\theta_B & 0 \\ 0 & 0 & 0 & 1 \end{bmatrix}, \tag{17}$$

is used. Here θ_B is the angle measured from the x_1 axis to the τ base vector for the surface at node B. In general, this can be written for all elements as

$$\mathbf{U} = \sum_{B=1}^{m} \mathbf{N}_B \, \mathbf{T}_B \, \mathbf{d}_B \,, \tag{18}$$

where the tangential and normal components of **d** for those nodes not on a solid surface would correspond to the Cartesian components, and the rotation matrices would simply be the identity matrix. For further details and discussions on the subject, see (Le Beau, 1990).

NUMERICAL EXAMPLES

We have tested our formulation on several steady-state problems. Here we present those for which shocks developed.

Reflection of a Shock Against a Wall

This problem is presented for several reasons. First, it possesses the features of an oblique shock, which has become a popular test problem in itself, plus a reflection point which will more critically test the accuracy of the method. A complete problem description can be found in Mallet (1985). A contour plot, a line plot at $y = 0.25$, and an elevation plot, all of density, are presented in Figures 1-3. This result is seen to be oscillation free, yet still maintains the structure of the upstream and reflected shocks.

Mach 0.84 Flow Past a Parabolic Arc Bump

The difficulty in solving transonic flow past the parabolic arc bump is due to the fact that a portion of the domain becomes supersonic and a shock wave forms on the surface of the bump. Thus even at a relatively modest Mach number of 0.84, the solution would have significantly poorer quality without the benefits of the shock capturing operator. The mesh used for this problem consists of 2068 elements over a 5% bump and is clustered in the direction of the bump. Figures 4-6 show line plots along the floor of the tunnel for pressure coefficient, as well as pressure contours in the area of the bump. The formation of a shock at approximately $x = 0.3$ is evident from both the line plots and the contour plot.

Mach 1.4 Flow Past a Parabolic Arc Bump

A more challenging problem for this algorithm exists in the analysis of supersonic flow past the parabolic arc bump. The mesh used for this problem consists of 2760 elements and 2883 nodes evenly distributed in a domain which has a bump height of 4%. Figures 7-9 show line plots at $y = 1.0$ and 0.5 for density, as well as pressure contours in the domain. This problem, which is similar to that analyzed in Shapiro (1988), creates an interesting shock interaction behind the bump. The shock from the leading edge of the bump is reflected down off the ceiling of the tunnel and crosses, then combines, with the shock formed at the trailing edge of the bump.

Mach 3.0 Flow Past a Circular Cylinder

The most challenging problem of this set is encountered when a cylinder is exposed to supersonic flow. The difficulties associated with this problem are the bow shock ahead of the cylinder and the near over expansion of the flow behind the cylinder. The domain is discretized by 4800 elements, 60 radially and 80 tangentially. The results, presented in Figures 10-15, show that most of the shock has been captured within two elements, as has the recompression of the flow behind the cylinder. In addition, the stagnation values and the stand-off distance of the shock are in good agreement with experimental results.

CONCLUDING REMARKS

In this work we have addressed some of the issues associated with the finite element solution of the Euler equations. These issues were related to the implementation of the slip boundary condition on solid walls and the ability of the method to successfully capture discontinuities in the solution field. We have shown that the implicit treatment of the no penetration boundary condition has many merits, making it virtually essential in formulations which ignore the viscous terms of the Navier-Stokes equations. The increased stability, and convergence rates, are well worth the extra cost associated with its implementation. We have also shown that the quality of the solutions obtained using conservation variables compares quite well with those obtained using entropy variables. In both variables, a proper shock capturing operator appears to be the crucial component in obtaining satisfactory results.

REFERENCES

Brooks, A.N. and Hughes, T.J.R., 1982, "Streamline Upwind/Petrov-Galerkin Formulations for Convection Dominated Flows with Particular Emphasis on the Incompressible Navier-Stokes Equations," *Computer Methods in Applied Mechanics and Engineering*, Vol. 32, pp. 199-259.

Hughes, T.J.R., Franca, L.P. and Hulbert, G.H., 1986, "A New Finite Element Formulation for Computational Fluid Dynamics: I. Symmetric Forms of the Compressible Euler and Navier-Stokes Equations and the Second Law of Thermodynamics," *Computer Methods in Applied Mechanics and Engineering*, Vol. 54, pp. 223-234.

Hughes, T.J.R. and Mallet, M., 1986, "A New Finite Element Formulation for Computational Fluid Dynamics: IV. A Discontinuity-Capturing Operator for Multidimensional Advective-Diffusive Systems," *Computer Methods in Applied Mechanics and Engineering*, Vol. 58, pp. 329-339.

Le Beau, G.J., 1990, "The Finite Element Computation of Compressible Flows," M.S. Thesis, University of Minnesota, Minneapolis, MN.

Li, C.P., 1986, "Computation of Three-dimensional Flow About Aerobrake Configurations," AIAA Paper 86-0566.

Mallet, M., 1985, "A Finite Element Method for Computational Fluid Dynamics," Ph.D. Thesis, Stanford University, Stanford, CA.

Shapiro, R., 1988, "An Adaptive Finite Element Solution Algorithm for the Euler Equations," Ph.D. Thesis, Massachusetts Institute of Technology, Cambridge, MA.

Tezduyar, T.E., and Hughes, T.J.R., 1982, "Development of Time-accurate Finite Element Techniques for First-order Hyperbolic Systems with Particular Emphasis on the Compressible Euler Equations," *Report prepared under NASA-Ames University Consortium Interchange*, No. NCA2-OR745-104.

Tezduyar, T.E., and Hughes, T.J.R., 1983, "Finite Element Formulations for Convection Dominated Flows with Particular Emphasis on the Compressible Euler Equations," *Proceedings, AIAA 21st Aerospace Sciences Meeting*, Reno, Nevada, AIAA Paper 83-0125.

Tezduyar, T.E., Glowinski, R., and Liou, J., 1988, "Petrov-Galerkin Methods on Multi-Connected Domains for the Vorticity-Stream Function Formulation of the Incompressible Navier-Stokes Equations," *International Journal of Numerical Methods in Fluids*, Vol. 8, pp. 1269-1290.

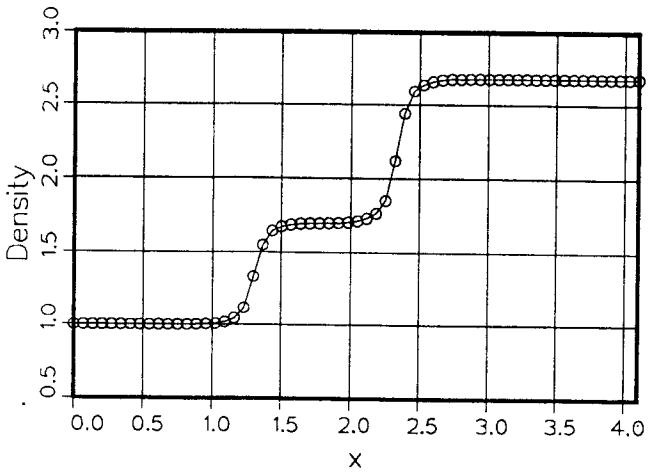

Figure 1. Density at y = 0.25, $M_\infty = 2.9$.

Figure 2. Pressure contours, $M_\infty = 2.9$.

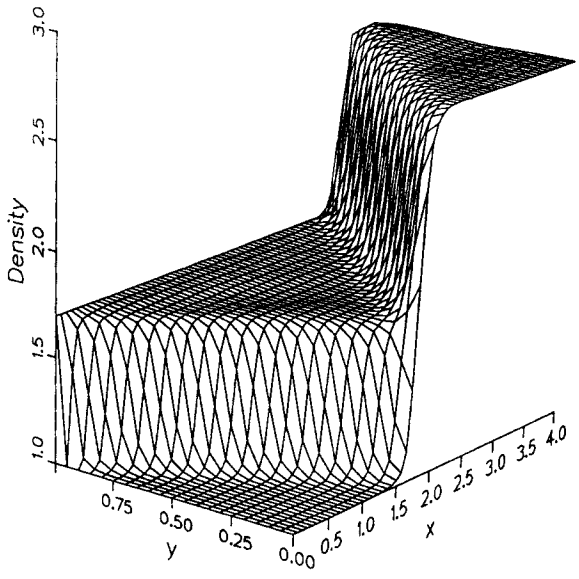

Figure 3. Elevation plot of the Density, $M_\infty = 2.9$.

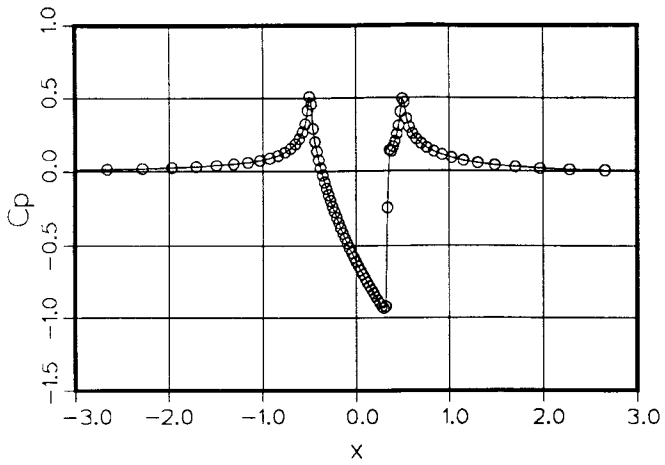

Figure 4. Pressure coefficient distribution on tunnel floor, $M_\infty = 0.84$.

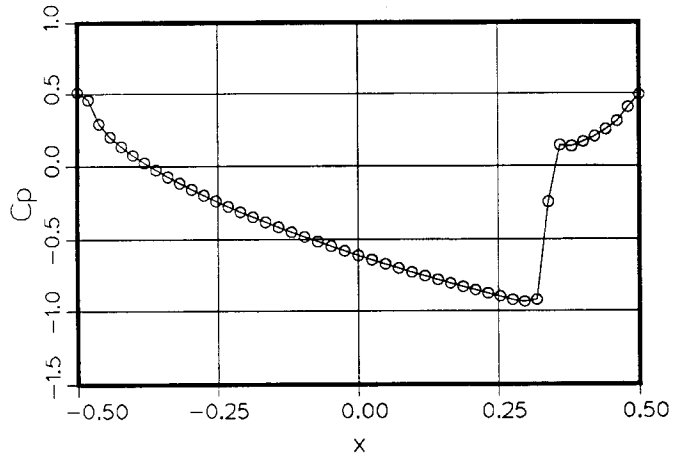

Figure 5. Pressure coefficient distribution on bump, $M_\infty = 0.84$.

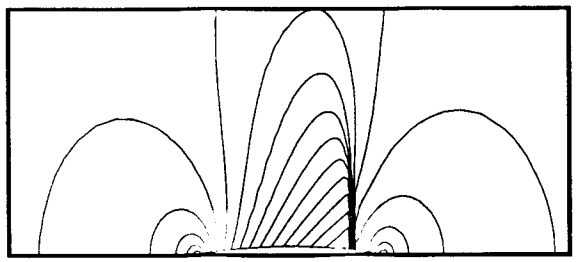

Figure 6. Pressure contours, $M_\infty = 0.84$.

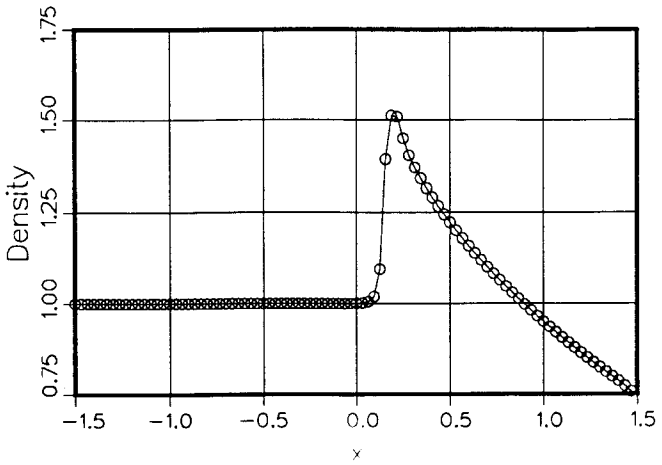

Figure 7. Density distribution on tunnel ceiling, $M_\infty = 1.4$.

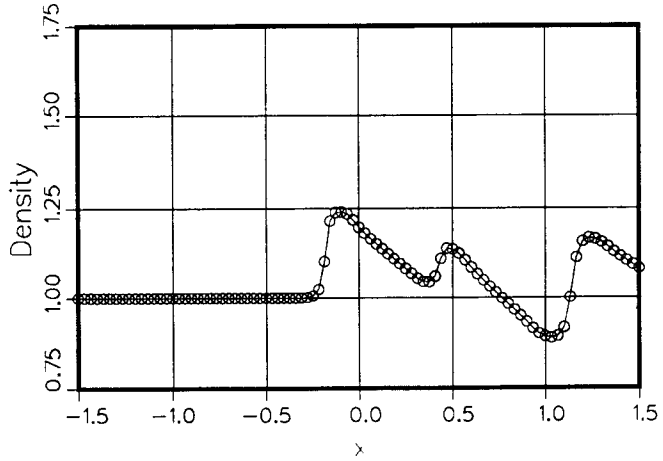

Figure 8. Density distribution along mid-point of tunnel, $M_\infty = 1.4$.

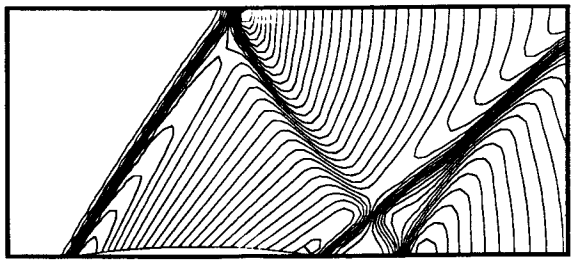

Figure 9. Pressure contours, $M_\infty = 1.4$.

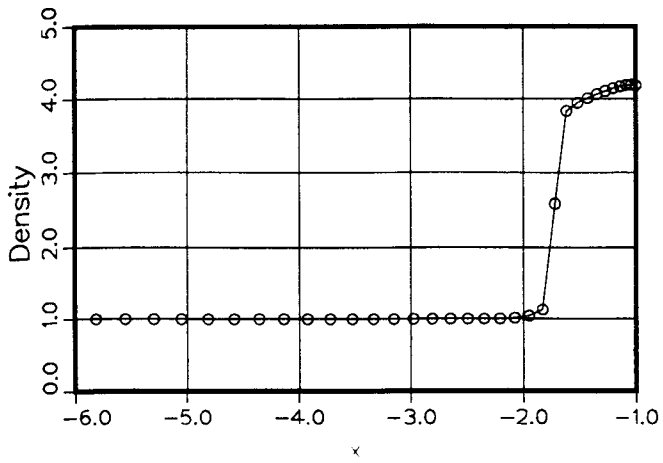

Figure 10. Density along symmetry axis ahead of cylinder, $M_\infty = 3.0$.

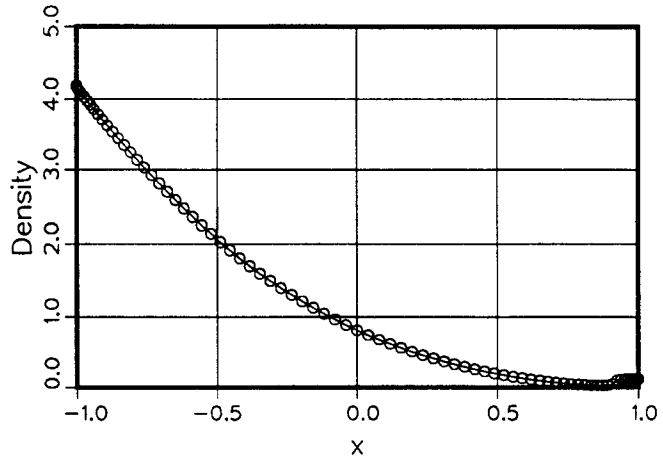

Figure 11. Density distribution on cylinder surface, $M_\infty = 3.0$

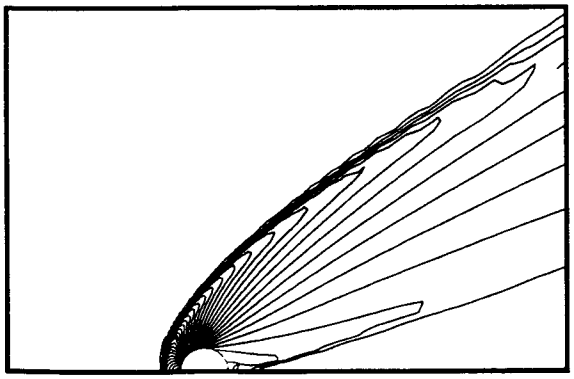

Figure 12. Pressure contours, $M_\infty = 3.0$.

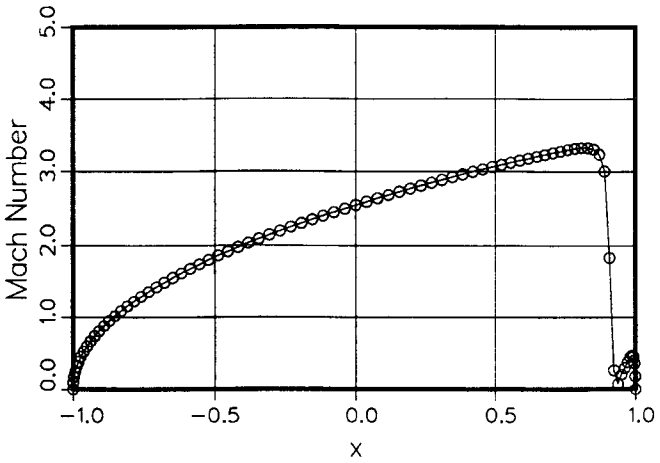

Figure 13. Mach number distribution on cylinder surface, $M_\infty = 3.0$.

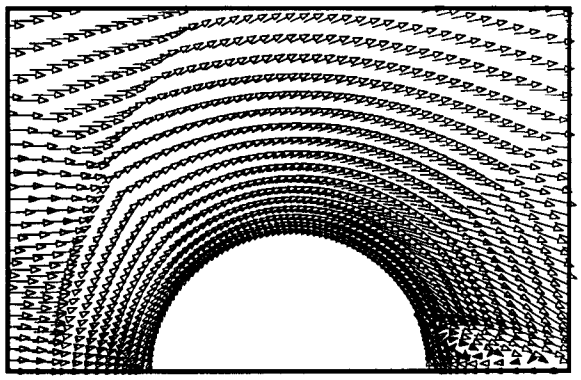

Figure 14. Velocity vectors, $M_\infty = 3.0$.

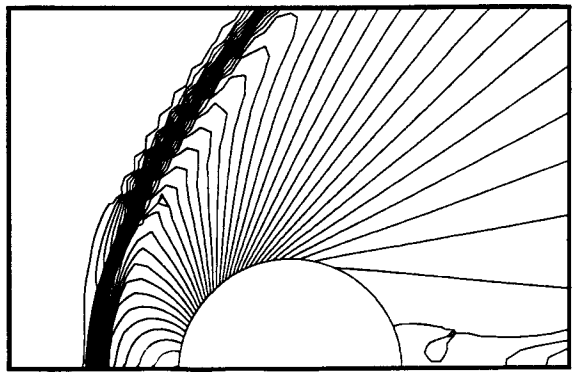

Figure 15. Pressure contours, $M_\infty = 3.0$.